# Flight-based Tuning of Trajectory Prediction Tool for Free-Flight Cargo Payloads

**Marwa Aly[1], M.Y.M. Ahmed [2] and M.Khalil[3]***

[1] M.Sc., Aerospace Engineering Department, Military Technical College, Egypt
[2] Professor, Aerospace Engineering Department, Military Technical College, Egypt
[3] Associate Professor, Aerospace Engineering Department, Military Technical College, Egypt

*E-mail: mostafa.samir@mtc.edu.eg

**Abstract.** Acquiring a reliable trajectory prediction tool is essential for designing and assessing free-flight flying objects of all types and ranges instead of expensive live firings. A "reliable" trajectory model should accurately predict the entire flight path of the free-flight object. Nonetheless, for simplicity, it may be adequate for some limitations for the model to be considered to define the key events of the flying object with good approximation as well as low cost. Free-flight cargo payloads are one sophisticated means for both civil and military applications. In the case of military applications, such as cargo missiles, the events of burnout and cargo dispensing are the two key events that control the overall performance of missiles in terms of dispensing range and cargo performance. The objective of the present paper is to develop and validate a robust trajectory prediction tool for free-flight cargo missiles. A six-degree-of-freedom (6-DOF) flight model is adopted to predict the trajectory of a test case cargo missile. To enhance the accuracy of trajectory prediction, the model is augmented with tuning parameters to account for uncertainties in missile motor thrust as well as aerodynamic forces. These parameters are evaluated by minimizing the deviation between the simulation data and live firings of the case study missile. Results show a significant improvement in prediction accuracy upon the addition of these tuning parameters.

**Keywords:**

Trajectory model, Firing Table, Fitting factors, Atmospheric parameters, Test-fire.

## 1. Introduction

The artillery firing tables are an important tool for artillery units for accurate and effective support firing; they provide the necessary information needed for firing elevation and azimuth adjustments for the accurate firing of artillery munitions for various ranges and under different environmental conditions.

The construction of firing tables [1] is based on extensive data such as missile mass properties, shooting angles, launching velocity, propulsive force, standard atmospheric conditions, and aerodynamic coefficients. All these data are used to establish numerical simulations that predict the missile trajectory. There are various mathematical models [2] that

can simulate the flying bodies starting with point mass to six-degrees-of-freedom (6-DOF) [3-6] according to the complexity needed. Based on firing data available at different flight conditions, these mathematical models are adopted to well simulate the flight performance, and hence the firing table is constructed including both standard and nonstandard flight conditions [1, 7].

For standard flight conditions, meteorological data are computed based on standards available from the literature such as the U.S. Standard Atmosphere 1962 [8, 9]. These meteorological data include the air pressure, temperature, and density as a function of the flight altitude. On the other hand, there are nonstandard conditions due to the real measurement of the environmental parameters such as air pressure, temperature, humidity, and wind speed and direction at different altitudes. These data can be collected pre-flight using a meteorological balloon with a radiosonde [10].

There is a difference between a simulation model and real fire due to approximations in mathematical models. This difference is obtained from the Doppler Tracking Radar [7] which is used to track the missile through the whole trajectory path and determine the corresponding velocity. Some simplifications and parameter limitations may be applied to the flight trajectory model due to the extensive flight trajectories needed to build such firing tables following some input data inaccuracies. Therefore, some correction factors [7, 11] are applied to create a correspondence between the simulated and the observed testing results.

The objective of the present study is multifold. Firstly, the launch elevations for the rocket weapon system (RWS) are determined based on predefined firing performance. Then, a comparison is conducted between results obtained using numerical simulations based on the 6-DOF trajectory model and real flight tests. A novel iterative process is developed to well estimate the fitting factors to best fit the trajectory model to the real flight test to apply it in the production process of artillery firing tables.

The rest of the paper is organized as follows: First, the case study missile is presented including its main dimensions and mass properties. Next, the research methodology is explained extensively. The key results are then proposed and discussed. Finally, the paper concludes the main findings.

## 2. Case Study

The case study considered through the proposed study is a fin-stabilized artillery rocket with a secondary munition (i.e. cargo) warhead as shown in Figure 1. To ensure the ground dispensing pattern in addition to the number of unexploded bomblets, a time fuse is implemented to achieve the recommended separation height. The rocket consists of four main sections, the mechanical electronic timed fuse (MENT), the cluster munitions including 54 bomblets, the dispensing mechanism, and the motor with a stabilizing unit. The main rocket characteristics are listed in Table 1. The thrust-time profile for the rocket motor, as illustrated in Figure 2, is achieved from a real static test, while the missile aerodynamic coefficients are estimated using the Missile DATCOM tool [4, 12].

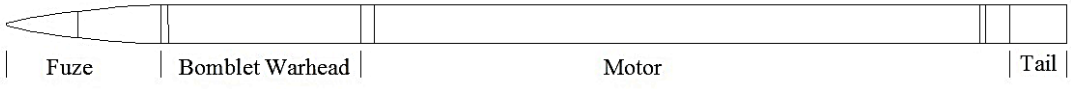


**Figure 1.** The case-study missile configuration.

**Table 1.** Rocket geometric and mass properties.

| No. | Parameter | | Value |
|---|---|---|---|
| 1 | Diameter | $D$ | 122 $mm$ |
| 2 | Overall Length. | $L_R$ | 3.3 $m$ |
| 3 | Total Mass. | $m_R$ | 70 $kg$ |
| 4 | Propellant Mass. | $m_p$ | 20.5 $kg$ |
| 5 | Propellant Burning Time. | $t_k$ | 2.3 s |
| 6 | Mean Thrust. | $T$ | 17600 $N$ |
| 7 | Launching velocity | $V_o$ | 26.7 $m/s$ |
| 8 | Launching spin rate | $p_o$ | 36 $rad/s$ |
| 9 | Initial $X_{cg}$ from the Nose Tip | $C.G\_x_i$ | 1.77 $m$ |
| 10 | Final $X_{cg}$ from the Nose Tip | $C.G\_x_f$ | 1.47 $m$ |
| 11 | Initial axial moment of inertia | $I\_xx_i$ | 0.1499 $kg.m^2$ |
| 12 | Final axial moment of inertia | $I\_xx_f$ | 0.1238 $kg.m^2$ |
| 13 | Initial lateral moment of inertia | $I\_yy_i = I\_zz_i$ | 41.58 $kg.m^2$ |
| 14 | Final lateral moment of inertia | $I\_yy_f = I\_zz_f$ | 33.83 $kg.m^2$ |

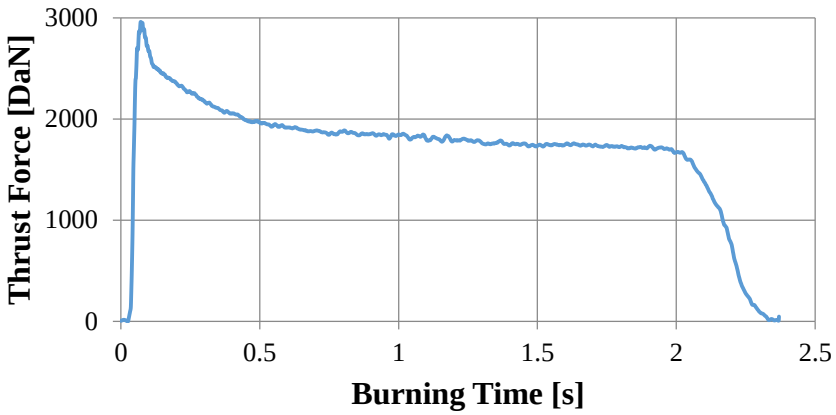


**Figure 2.** Thrust-time profile for the case-study.

## 3. Methodology

Firing table (FT) accuracy is based mainly on the quality of input data used regarding the missile as well as the launching process, the applied trajectory model used, and the number of firings implemented to improve the mathematical model used to produce FT.

In this study, different fitting factors are adopted through different flight phases including boosting and coasting flight phases [11]. As illustrated in Figure 3, there are three points on the trajectory to be a reference, namely the muzzle (A), burn-out point (B), and separation point (C).

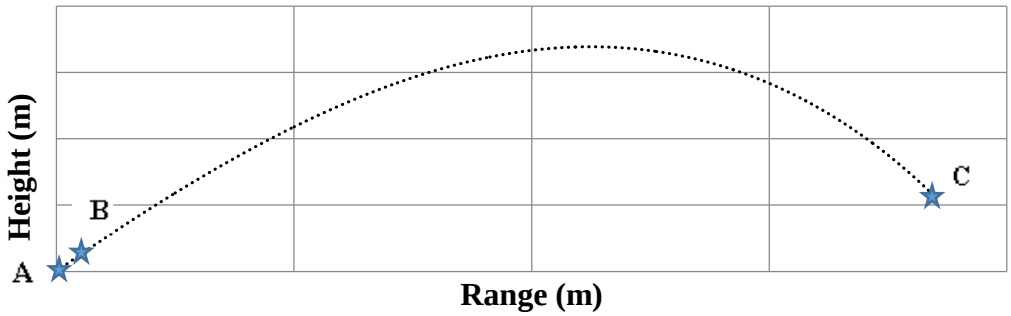


**Figure 3.** Schematic of the missile trajectory from launch to separation point.

*3.1 Trajectory model*

To provide an accurate representation of flying body motion assuming a rigid body that possesses three position and three orientation degrees of freedom, a 6-DOF trajectory model is utilized considering non-rotating flat earth and following the forces and moments representation as illustrated in Figure 4 including motor thrust and the aerodynamic forces and moments.

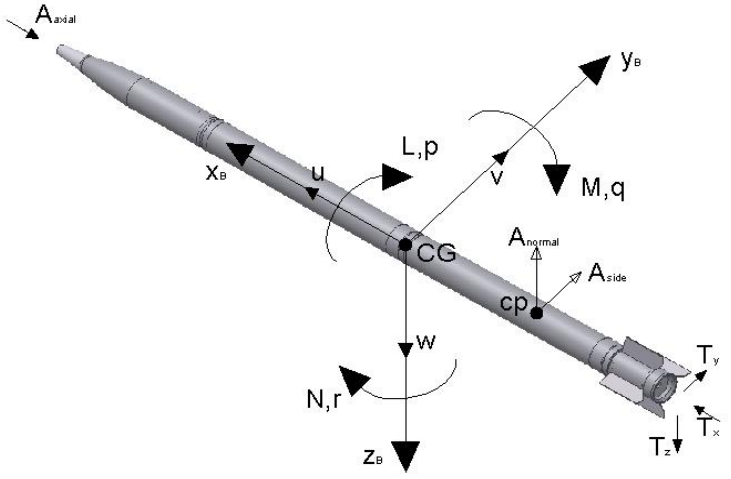


**Figure 4.** Forces and moments applied on the flying body.

A complete set of equations relating forces and moments to linear and angular motions are derived as follows[3],

$$\begin{bmatrix}\dot{u}\\ \dot{v}\\ \dot{w}\end{bmatrix} = \left(\frac{1}{m}\right)\begin{bmatrix}T_x - A_{axial}\\ T_y + A_{side}\\ T_z - A_{normal}\end{bmatrix} + g\begin{bmatrix}-\sin\theta\\ \cos\theta\,.\sin\phi\\ \cos\theta\,.\cos\phi\end{bmatrix} + \begin{bmatrix}p_B^E + p\\ q_B^E + q\\ r_B^E + r\end{bmatrix} \times \begin{bmatrix}u\\ v\\ w\end{bmatrix} \tag{1}$$

$$\begin{aligned}\dot{p} &= \left(\frac{1}{I_x I_z - I_{zx}^2}\right).\left[I_z.L + I_{zx}.N + I_z.I_{zx}\left(1 + \frac{I_x - I_y}{I_z}\right).p.q + \left(I_y I_z - I_z^2 - I_{zx}^2\right).q.r\right]\\ \dot{q} &= \left(\frac{M}{I_y}\right) + \left(\frac{I_{zx}(r^2 - p^2) + (I_z - I_x).r.p}{I_y}\right)\\ \dot{r} &= \left(\frac{1}{I_x I_z - I_{zx}^2}\right).\left[I_{zx}.L + I_x.N + \left(I_y - I_x - I_z\right).I_{zx}.r.q + \left(I_x^2 - I_x I_y + I_{zx}^2\right).q.p\right]\end{aligned} \tag{2}$$

where, $x$, $y$, and $z$ are the body fixed reference frame. u, v, and w are the three components of the linear velocity of the body in the body-fixed reference frame. $p$, $q$, and $r$ are the three components of the angular velocity of the body in the body-fixed reference frame. $T_x$, $T_y$, and $T_z$ are the three components of the resultant external force acting on the body in the body-fixed reference frame. $L$, $M$, and $N$ are the three components of resultant external moments acting on the body in the body-fixed reference frame. $I_x$, $I_y$, and $I_z$ are the centroidal mass moment of inertia of the body about the body-fixed reference frame. $I_{zx}$ is the centroidal mass product of the inertia of the body. $\varphi$, $\theta$, and $\psi$ are the Euler angles namely the roll, elevation, and azimuth angles respectively.

While the relationship between the non-inertial angular rates and the time rate of change of the Euler angles are [3],

$$\begin{bmatrix} \dot{\phi} \\ \dot{\theta} \\ \dot{\psi} \end{bmatrix} = \begin{bmatrix} 1 & \sin\phi \tan\theta & \cos\phi \tan\theta \\ 0 & \cos\phi & -\sin\phi \\ 0 & \sin\phi \sec\theta & \cos\phi \sec\theta \end{bmatrix} \begin{bmatrix} p \\ q \\ r \end{bmatrix} \tag{3}$$

Finally, the body's ground speed can be determined as,

$$\begin{bmatrix} v_x \\ v_y \\ v_z \end{bmatrix}_E = \begin{matrix} \cos\theta\cos\psi & \begin{pmatrix} \sin\phi\sin\theta\cos\psi \\ -\cos\phi\sin\psi \end{pmatrix} & \begin{pmatrix} \cos\phi\sin\theta\cos\psi \\ +\sin\phi\sin\psi \end{pmatrix} \\ \cos\theta\sin\psi & \begin{pmatrix} \sin\phi\sin\theta\sin\psi \\ +\cos\phi\cos\psi \end{pmatrix} & \begin{pmatrix} \cos\phi\sin\theta\sin\psi \\ -\sin\phi\cos\psi \end{pmatrix} \\ -\sin\theta & \sin\phi\cos\theta & \cos\phi\cos\theta \end{matrix} \begin{bmatrix} v_x \\ v_y \\ v_z \end{bmatrix}_{\boldsymbol{B}} \tag{4}$$

*3.2 Test-fire setup*

Artillery test-fire is a crucial procedure to improve the accuracy of the flight simulations and hence increase the accuracy of the produced FT and enhance overall combat readiness. The test-fire setup procedure is a meticulously planned and executed process that involves numerous steps to ensure safety, accuracy, and consistency in the testing environment. From site preparation to data analysis, each phase of the test-fire procedure is essential for obtaining reliable results and informing future decisions in artillery operations. The firing setup for artillery involves several procedures such as:

- Site setup, by deploying the launcher in the firing direction, ensuring it is stable and properly aligned;
- Ground meteorological station, is a facility equipped with instruments to measure atmospheric parameters such as surface temperature, pressure, humidity, wind speed, and wind direction;
- A meteorological balloon with a radiosonde, is a balloon equipped with a radiosonde to measure and record atmospheric parameters such as temperature, pressure, humidity, wind speed, and wind direction;
- Preparing the ammunition, by conditioning the missiles at 15°C for 8 hours before firing;
- Aiming and alignment, by considering the metrological deviation from standard to calculate the corrections needed to adjust the final aiming angles (elevation and azimuth);
- Firing the missiles in sequence with known weight;

- Finally, monitor the missile's flight trajectory to record relevant data, such as muzzle velocity, burn-out velocity and location, point of separation, and impact point.

Then, to well capture the flight performance during different flight phases, some facilities are used to enhance and assess the quality of the produced FT as follows:

- High-speed Camera, which is an important tool used to capture a high-quality video of the missile at launching to observe the attitude velocity of the missile at the muzzle;
- Doppler Tracking Radar, which is used to track the missile through the whole trajectory path, and determine the corresponding velocity;
- Field observation, where field observers can visually identify the separation and impact points and the corresponding flight time. For observers' safety, the observation point should be no less than 2 km away from the predicted impact point.

*3.3 Deduction of fitting factors*

As shown in Figure 3, through the active-flight phase (i.e. portion AB, from muzzle till the burn-out point) the dominant factors are the motor thrust $T$ and the aerodynamic lift force coefficient $C_L$ (i.e. source of the static stability $SS$). Hence, any deviation from real-flight in point B (i.e. the burn-out point), can be adapted by tuning both the motor thrust that impacts the burn-out velocity and $C_L$ that impacts the burn-out altitude $Z_{bo}$ in the presence of surface-wind. For the flight portion BC, which represents the missile flight from the burn-out point B to the cargo separation point C, the dominant factor is the missile's aerodynamic drag force coefficient $C_{D,m}$. Therefore any deviation from real-flight in point C (i.e. separation point) can be tuned using the missile's $C_D$.

Herein, to adapt the motor thrust, a thrust factor $F_b$ is applied to adjust the thrust value, ensuring that the simulated burn-out velocity fits the measured real flight data. Similarly, a lift factor $F_l$ is implemented to tune the resultant $C_L$ through the boost phase that fits the simulated altitude/drift at the burn-out point with the actual flight measurement. Finally, a drag factor $K_i$ is employed to minimize the discrepancy between the real flight range of the missile at the cargo separation point C, and the simulated data obtained. For different firing elevations $\theta$, fitting equations are utilized to deduce the corresponding polynomial coefficients based on the data measured as listed in Table 2. Figure 5 outlines the iterative process used to determine the thrust factor $F_b$, lift factor $F_l$, and drag factor $K_i$. This process involves two phases $F_b$ and $F_l$ are for the active phase while $K_i$ is for the passive phase. The method ensures that simulated parameters including burn-out velocity, altitude, drift, and missile range align with real flight data by systematically adjusting these factors.

**Table 2.** List of the proposed fitting factors.

| No. | Flight phase | Measured parameter | Tunned parameter | Fitting equation |
|---|---|---|---|---|
| 1 | Active, AB | Missile's velocity $V$ | $V_{bo}$ | $F_b = a_{0,1} + a_{1,1}.\theta + a_{2,1}.\theta^2$ |
| | | Missile's altitude $Z$ | $C_L$ | $F_l = a_{0,2} + a_{1,2}.\theta + a_{2,2}.\theta^2$ |
| 2 | Passive, BC | Missile's range $R$ | $C_{D,m}$ | $K_i = a_{0,3} + a_{1,3}.\theta + a_{2,3}.\theta^2$ |

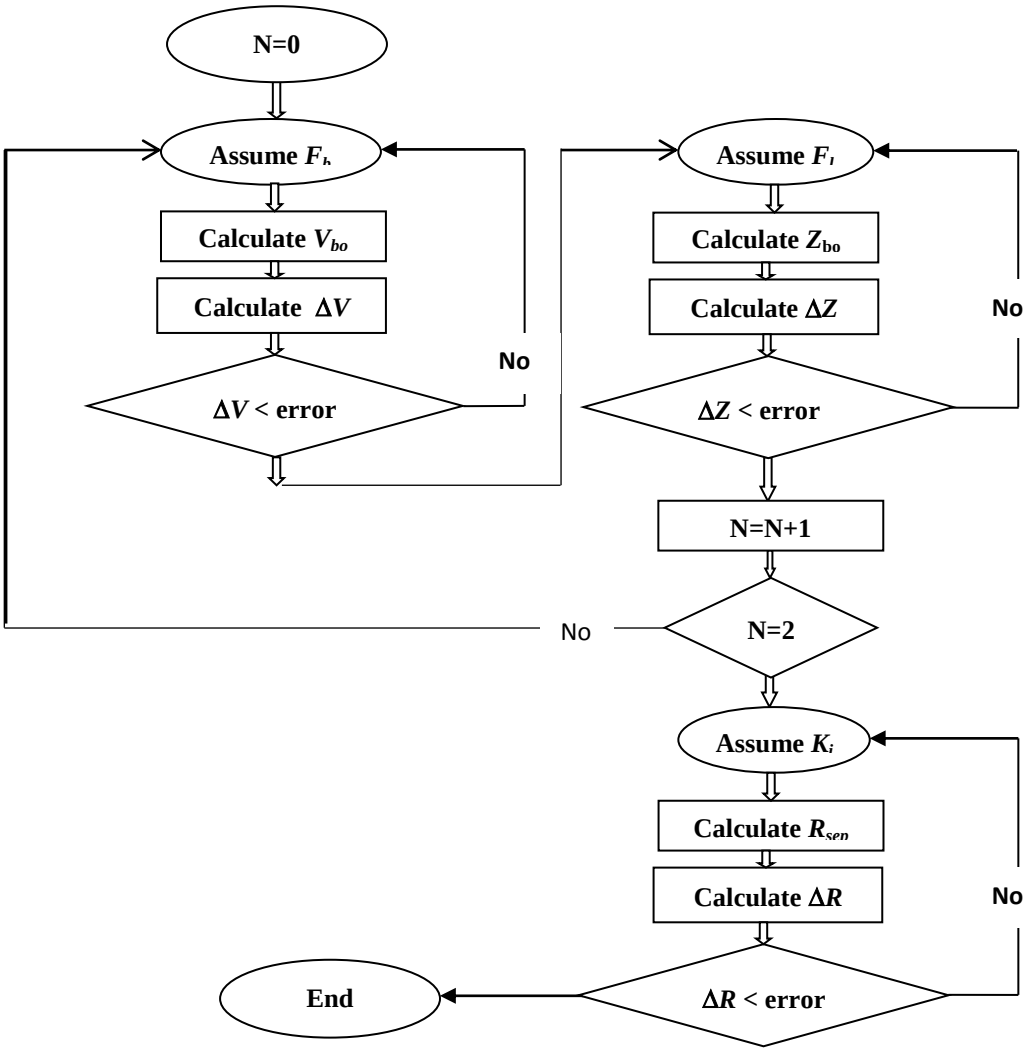


**Figure 5.** Flow Chart for fitting factors estimation process.

## 4. Results and Discussions

Based on simulation results for three different missile ranges representing a minimum of 6 km, mid of 12 km, and a maximum of 18 km, with a cargo warhead separation at an altitude of 2350m, a total of 17 test shots are planned. These tests correspond to three different launch elevations $\theta$ as listed in Table 3 including the number of shots done for each elevation.

**Table 3.** Test setup.

| | $\theta$ [deg] | No of Shots |
|---|---|---|
| **Max. Range** | 45.6 | 7 |
| **Mid. Range** | 25.3 | 7 |
| **Min. Range** | 28.7 | 3 |

Figure 6 illustrates the differences between simulated and real flight trajectories. Real flight data is categorized into three groups, as listed in Table 3. For each group, only the shots with the maximum and minimum ranges are shown in Figure 6, except for the minimum range group, where the tracking radar data for the other two shots is not successfully recorded. The simulated trajectory is based on nominal missile characteristics including the estimated aerodynamic coefficients using Missile Datcom, the nominal thrust profile, and standard atmospheric conditions. In contrast, real flight data accounts for actual thrust variations, nonstandard meteorological conditions (such as temperature, pressure, wind speed, and wind direction), and other discrepancies in shape and mass properties from their nominal values. Table 4 summarizes the key variables that contribute to the differences between the simulations and the average of real flight data namely the missile burn-out velocity and altitude, and the separation point downrange.

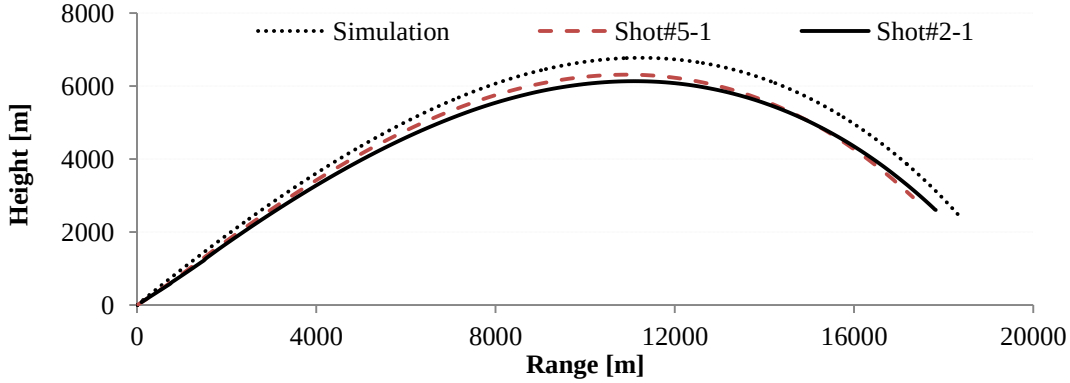


(a) Max Range (shots# 2 and 5)

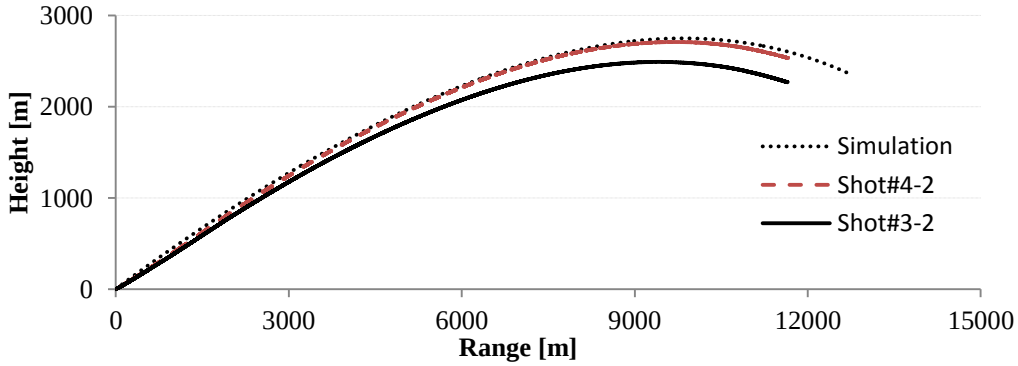


(b) Mid Range (shots# 3 and 4)

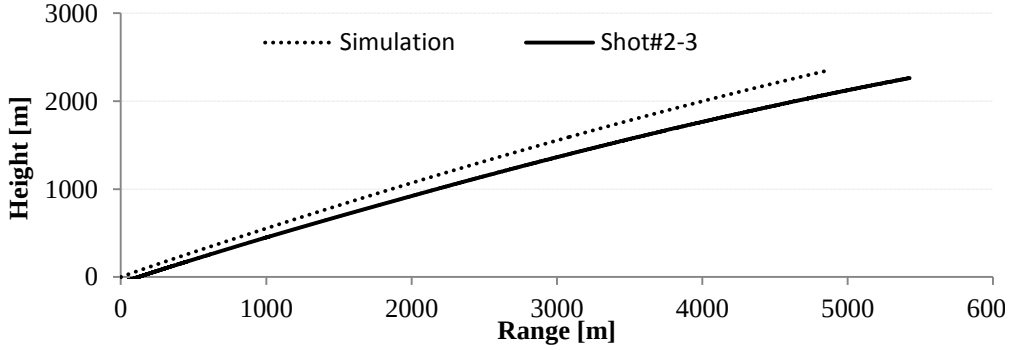


(c) Min Range

**Figure 6.** Trajectory results for three ranges.

**Table 4.** Results for both simulations and test flights.

| $\theta$ [deg] | Burn out point | | | | Separation point | |
|---|---|---|---|---|---|---|
| | $V_{bo}$ [m/s] | | Altitude [m] | | Range [m] | |
| | Sim. | Exp. | Sim. | Exp. | Sim. | Exp. |
| 45.6 | 662.67 | 628.4 | 608 | 580 | 17876 | 17406 |
| 25.3 | 669.6 | 650 | 342 | 338 | 12042 | 11520 |
| 28.7 | 668 | 650.5 | 391 | 387 | 5504 | 5260 |

To compute the fitting factors to best fit the simulations (Sim.) with experimental data (Exp.), the average of key parameters representing all real shoots per elevation is calculated including the burn-out velocity, burn-out altitude, and separation range as listed in Table 4. Applying the iterative process shown in Figure 5, the three fitting factors needed to best fit the key flight parameters in both simulation and real flight are estimated as listed in Table 5. These fitting factors are expressed as polynomial functions of the launch elevation $\theta$, as proposed in Table 2. Hence, utilizing the three estimated values for each fitting factor, the polynomial coefficients of each polynomial function are determined as listed in Table 6.

**Table 5.** Fitting factors results.

| $\theta$ [deg] | $F_b$ | $F_l$ | $K_i$ |
|---|---|---|---|
| 45.6 | 0.94695 | 40 | 0.944 |
| 25.3 | 0.96985 | 37.2 | 1.0555 |
| 28.7 | 0.9726 | 42 | 1.1385 |

**Table 6.** Polynomial coefficients results.

| Fitting factor | *Polynomial coefficients* | | |
|---|---|---|---|
| | $a_0$ | $a_1$ | $a_2$ |
| $F_b$ | 0.866 | 0.400967 | –0.37626 |
| $F_l$ | –53.253 | 314.11 | –247.4507 |
| $K_i$ | –0.8471 | 6.87381 | –5.8091 |

## 5. Conclusions

Due to mathematical model simplifications and uncertainties in the information available for missiles as a case study, some discrepancies between the simulation model and real flight tests arise. To minimize these differences, corrections are necessary to best align numerical trajectory simulation results with the real flight tests. This study proposed a novel estimation process for some correction factors that improve the accuracy of trajectory simulations before the production of artillery firing tables. By systematically tuning the thrust factor, lift factor, and drag factor through an iterative fitting process, the computed missile performance is better aligned with measure firing test results. The proposed approach reduces errors in key flight parameters, such as burn-out velocity, burn-out altitude, and overall missile range that can be implemented to produce a mathematical model that best performs the trajectory parameters for a range of launching elevations. Future work may involve extending the correction methodology further by incorporating the flight phase extends from the cargo separation till the ground impact.

## References


[1] Mady, M., Khalil, M., and Yehia, M., "Modelling and Production of Artillery Firing-Tables: Case-Study," in *Journal of Physics: Conference Series*, 2020, p. 082043.

[2] R.L., M. *Modern Exterior Ballistics: The Launch and Flight Dynamics of Symmetric Projectiles*: Schiffer Publishing, 1999.

[3] Khalil, M., Abdalla, H., and Kamal, O., "Trajectory Prediction for a Typical Fin Stabilized Artillery Rocket," in *International conference on aerospace sciences and aviation technology*, 2009, pp. 1-14.

[4] Bashir, M., Khan, S. A., Udayagiri, L., and Noor, A., "Dynamic Stability of Unguided Projectile with 6-Dof Trajectory Modeling," in *2017 2nd International Conference for Convergence in Technology (I2CT)*, 2017, pp. 1002-1009.

[5] Chusilp, P., and Charubhun, W., "Estimation of Impact Points of an Artillery Rocket Fitted with a Non-Standard Fuze," in *2016 Second Asian Conference on Defence Technology (ACDT)*, 2016, pp. 25-31.

[6] Charubhun, W., Chusilp, P., and Nutkumhang, N., "Effects of Aerodynamic Coefficient Uncertainties on Trajectory Simulation of a Short-Range Solid Propellant Free Rocket," in *26th International Symposium on Ballistics*, 2011, pp. 12-16.

[7] Khalil, M. "Study on Modeling and Production Inaccuracies for Artillery Firing," *Archive of mechanical engineering*, 2022, pp. 165-183-165-183.

[8] "U.S. Standard Atmosphere," U.S. Committee on Extension to the Standard Atmosphere, Washington, D.C1962.

[9] *Manual of the Icao Standard Atmosphere: Extended to 80 Kilometres*: International Civil Aviation Organization, 1993.

[10] Ivan, J., Sustr, M., Sládek, D., Varecha, J., and Gregor, J., "Emergency Meteorological Data Preparation for Artillery Operations," in *ICINCO (1)*, 2023, pp. 250-257.

[11] NATO. "Stanag 4355–the Modified Point Mass and Five Degrees of Freedom Trajectory Models." 2009, p. 95.

[12] Chusilp, P., Charubhun, W., and Nutkumhang, N., "A Comparative Study on 6-Dof Trajectory Simulation of a Short Range Rocket Using Aerodynamic Coefficients from Experiments and Missile Datcom," in *The Second TSME International Conference on Mechanical Engineering*, 2011, pp. 19-21.